Spectroscopic Properties of the Main-Form and High-Salt Peridinin−Chlorophyll *a* Proteins from *Amphidinium carterae*[†]

Robielyn P. Ilagan,[‡] Sumie Shima,[‡] Alexander Melkozernov,[§] Su Lin,[§] Robert E. Blankenship,[§] Frank P. Sharples,[||] Roger G. Hiller,[||] Robert R. Birge,*[,‡] and Harry A. Frank*[,‡]

Department of Chemistry, 55 North Eagleville Road, University of Connecticut, Storrs, Connecticut 06269-3060, Department of Chemistry and Biochemistry, Arizona State University, Tempe, Arizona 85287-1604, and School of Biological Sciences, Macquarie University, NSW 2109, Australia

Received October 4, 2003; Revised Manuscript Received December 5, 2003

ABSTRACT: The main-form (MFPCP) and high-salt (HSPCP) peridinin−chlorophyll *a* proteins from the dinoflagellate *Amphidinium carterae* were investigated using absorption, fluorescence, fluorescence excitation, two-photon, and fast-transient optical spectroscopy. Pigment analysis has demonstrated previously that MFPCP contains eight peridinins and two chlorophyll (Chl) *a* molecules, whereas HSPCP has six peridinins and two Chl *a* molecules [Sharples, F. P., *et al*. (1996) *Biochim. Biophys. Acta 1276*, 117−123]. Absorption spectra of the complexes were recorded at 10 K and analyzed in the 400−600 nm region by summing the individual 10 K spectra of Chl *a* and peridinin recorded in 2-MTHF. The absorption spectral profiles of the complexes in the Q_y region between 650 and 700 nm were fit using Gaussian functions. The absorption and fluorescence spectra from both complexes exhibit several distinguishing features that become evident only at cryogenic temperatures. In particular, at low temperatures the Q_y transitions of the Chls bound in the HSPCP complex are split into two well-resolved bands. Fluorescence excitation spectroscopy has revealed that the peridinin-to-Chl *a* energy transfer efficiency is high (>95%). Transient absorption spectroscopy has been used to measure the rate of energy transfer between the two bound Chls which is a factor of 2.9 slower in HSPCP than in MFPCP. The kinetic data are interpreted in terms of the Förster mechanism describing energy transfer between weakly coupled, spatially fixed, donor−acceptor Chl *a* molecules. The study provides insight into the molecular factors that control energy transfer in this class of light-harvesting pigment−protein complexes.

The water-soluble peridinin−chlorophyll *a* protein (PCP)[1] from the dinoflagellate *Amphidinium carterae* harvests light very efficiently (*1*−*4*). The process is facilitated by closely associated peridinins and chlorophylls (Chl) bound to a 32 kDa protein subunit. X-ray crystallography at a resolution of 2.0 Å has revealed a trimeric structure of subunits (*5*, *6*). Eight peridinins and two Chls are bound noncovalently in an approximate C_2 symmetrical arrangement in the hydrophobic folds of each individual subunit (Figure 1). The peridinins are assembled in groups of four within each subunit, and each group is clustered around and in van der Waals contact with the π-electron system of one Chl. The two Chl molecules within each subunit have a center-to-center distance of 17.4 Å. The shortest distance between Chls in neighboring subunits is ∼40 Å.

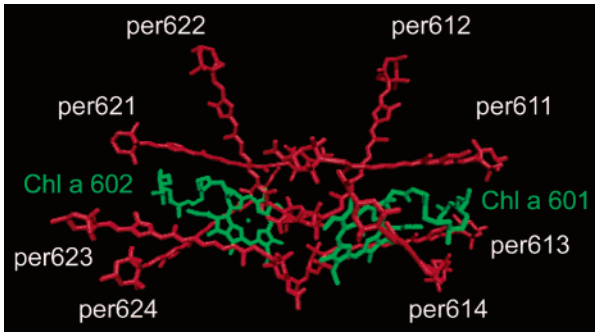

FIGURE 1: Structure of the pigments in a monomeric subunit of the MFPCP complex. It is comprised of two Chl *a* and eight peridinin (per) molecules. The coordinates of the structure were taken from the Brookhaven Protein Data Bank (entry 1PPR).

Absorption, fluorescence, linear dichroism, circular dichroism (CD), two-photon excitation, and transient optical spectroscopic studies of the PCP complex at room and cryogenic temperatures have revealed the electronic configurations of the excited states of the bound peridinins, the nature of the interactions between the pigments, and the

[†] This work was supported by grants from the National Institutes of Health (GM-34358 to R.R.B. and GM-30353 to H.A.F.), the National Science Foundation (EIA-0129731 to R.R.B., MCB-9727607 to R.E.B., and MCB-9816759 to H.A.F.), the University of Connecticut Research Foundation (to H.A.F.), the Department of Agriculture (NRICGP/USDA 2003-35318-13665 to A.N.M.), and the Australian Research Council (A00000264 to R.G.H.).

* To whom correspondence should be addressed: Department of Chemistry, 55 N. Eagleville Rd., University of Connecticut, Storrs, CT 06269-3060. Telephone: (860) 486-2844. Fax: (860) 486-6558. E-mail: harry.frank@uconn.edu or rbirge@uconn.edu.

[‡] University of Connecticut.

[§] Arizona State University.

[||] Macquarie University.

[1] Abbreviations: CD, circular dichroism; Chl, chlorophyll; DAS, decay-associated spectra; fwhm, full width at half-maximum; HSPCP, high-salt peridinin−chlorophyll *a* protein; MFPCP, main-form peridinin−chlorophyll *a* protein; PCP, peridinin−chlorophyll *a* protein; TPE, two-photon excitation.

10.1021/bi0357964 CCC: $27.50
Published on Web 01/24/2004

dynamics and efficiency of singlet and triplet energy transfer (*2*−*4*, *7*−*20*). Quantum mechanical computations have used the high-resolution structure of the PCP complex to clarify the molecular basis of structural stabilization (*21*), to examine the nature of the excited states of the bound peridinins (*19*, *22*), and to identify the mechanism and pathways of energy flow through this protein and onward to the membrane-bound light-harvesting proteins and ultimately to photosystem II (*8*, *10*).

Studies on the native PCP and on the isolated pigments in various solvents have shown that light absorption by peridinin involves a strongly allowed optical transition from the ground state (S_0) to an excited state (S_2). The CD data and computations suggest that the S_2 states of the peridinins are exciton-coupled and share excitation in this manner prior to transferring the energy to Chl (*4*, *7*, *8*, *10*, *11*, *19*, *20*). The S_2 state of peridinin decays on an ∼100 fs time scale to a low-lying S_1 state whose population from the ground state is forbidden by symmetry (*2*, *4*, *23*). The lifetime of the S_1 state of peridinin in solution is strongly dependent on the polarity of the solvent, and ranges from ∼7 ps in the strongly polar solvent methanol to ∼160 ps in nonpolar solvents such as CS_2 (*9*, *17*, *23*). The initial explanation for this behavior invoked the presence of a discrete charge transfer state in the excited state manifold of peridinin along with S_1 and S_2 (*17*), and a recent computational study supports this model (*22*). However, other experimental investigations using time-resolved and two-photon methods have suggested an alternative interpretation in which the S_1 state itself possesses substantial charge transfer character due to the carbonyl moiety conjugated with the polyene chain (*19*, *23*). In this model, large polarity-induced changes in the charge transfer character in both S_1 and S_0 are thought to account for the solvent dependence of the spectroscopic properties and excited state dynamics of peridinin.

Given the complex nature of the electronic states of peridinin in solution, it is not surprising that the mechanism of energy transfer from the peridinins to Chl in the PCP complex is not yet clear. Early time-resolved transient absorption spectroscopic investigations suggested essentially all of the energy was transferred to Chl via the S_1 state of peridinin (*3*), and this was supported by structure-based quantum mechanical calculations on the protein (*10*). However, more recent femtosecond time-resolved transient absorption data have suggested that anywhere from 25 to 50% of the energy arriving on Chl may be transferred via the S_2 state of peridinin (*4*, *24*, *25*).

The steady state absorption spectrum of the PCP complex exhibits features that are predominantly associated with the peridinins in the region of 400−550 nm and the Chls near 438 nm (Soret) and 670 nm (Q_y). Spectroscopic analyses indicate spectral inhomogeneity among pigments bound in the complexes (*11*, *26*−*28*). Deconvolution of the low-temperature absorption spectrum of the PCP complex using spectra obtained for the individual pigments in solution reveals three different pairs of peridinin spectra having $S_0 \rightarrow S_2$ origins at 545, 528, and 523 nm (*19*). The pairs may belong to equivalent peridinins occupying C_2 symmetric sites in the protein subunit. The two remaining peridinins are not spectrally equivalent and have blue-shifted origins at 485 and 465 nm. MNDO-PSDCI computations based on the coordinates derived from the crystal structure suggest that these are peridinins per612 and per622 [in the notation of Damjanovic *et al.* (*10*), or Per2 and Per2′, respectively, using the notation of Hofmann *et al.* (*5*)], and that the spectra from the chromophores occupying these sites not only are blue-shifted but also have inverted S_1 and S_2 states. This finding lends support to the model proposed by Damjanovic *et al.* (*10*) in which because of non-optimal orientation factors and high site energies, per612 and per622 transfer energy to other peridinins rather than directly to Chl.

During purification of the PCP complex using a linear salt gradient and cation-exchange column chromatography, a divergent form comprising ∼2% of the total PCP was eluted at high salt concentrations (*29*). This new form of PCP is distinguished from the main-form PCP (hereafter denoted MFPCP) by differences in spectral properties, pigment stoichiometry, molar mass, antigenicity, and amino acid sequence (*29*). The sequence of the variant PCP, denoted high-salt PCP (HSPCP), is 31% homologous with that of the MFPCP complex, and HSPCP retains a two-subunit domain structure; however, it binds six peridinins instead of eight and has a molar mass of 34 kDa, versus a mass of 32 kDa for MFPCP (*29*). The differences in pigment stoichiometry and spectral properties between MFPCP and HSPCP make a comparative investigation of the two complexes highly desirable.

In this work, absorption, fluorescence, fluorescence excitation, two-photon excitation, and transient optical spectroscopic studies of the HSPCP complex at room and cryogenic temperatures are presented. The results are compared with those obtained from studies on the MFPCP complex reported here and previously in the literature and are used to further our understanding of the molecular basis for the high energy transfer efficiency achieved by this class of photosynthetic light-harvesting complexes.

MATERIALS AND METHODS

Sample Preparation

The MFPCP and HSPCP complexes were prepared as described by Sharples *et al.* (*29*). Briefly, *A. carterae* was cultured in Provasoli's enriched seawater at a light intensity of 20 μmol m^{-2} s^{-1}. The cells were precipitated in 0.5 mM $AlK(SO_4)_2 \cdot 12H_2O$, centrifuged, and washed with 50 mM Tricine/20 mM KCl buffer (pH 7.5). The cells were ruptured using a French pressure apparatus at 80 MPa followed by centrifugation to remove the debris and membranes. The PCP complex was obtained by fractionation of the supernatant in 70−90% ammonium sulfate. The complex was then dialyzed against 5 mM sodium acetate (pH 5.0) and further purified on a CM Tris-acryl column using a linear NaCl gradient. A major PCP complex, main-form PCP (MFPCP), was eluted between 0.05 and 0.15 M NaCl with an A_{478}/A_{280} ratio of >4.5, while a minor PCP, high-salt PCP (HSPCP), was eluted at 0.25 M NaCl. The purity and homogeneity of the samples were determined using SDS−polyacrylamide gel electrophoresis. The purified MFPCP and HSPCP were stored in 50 mM Tricine, 20 mM KCl, and NaN_3 buffer (pH 7.5) in the dark at −24 °C until they were ready for use in the spectroscopic experiments.

Spectroscopic Methods

Absorption, Fluorescence, and Fluorescence Excitation Spectroscopy. Absorption spectra of MFPCP and HSPCP were recorded at room temperature, 77 K, and 10 K on samples held in 1 cm × 1 cm polymethacrylate plastic cuvettes using a Cary 50 UV−vis spectrometer. Absorption spectroscopy was performed at 77 K using a quartz dewar filled with liquid nitrogen and at 10 K using a Janis helium vapor flow model STVP100 cryostat. The MFPCP and HSPCP complexes were suspended in 50 mM Tricine/20 mM KCl buffer (pH 7.5) which contained 50% glycerol for the 10 K experiment and 60% glycerol for the 77 K experiment.

The fluorescence and fluorescence excitation spectra of the MFPCP and HSPCP complexes were recorded on a Jobin Yvon Horiba Fluorolog-3 model FL3-22 spectrofluorometer at room temperature and 77 K. The spectrofluorometer is equipped with 450 W ozone-free xenon lamp and a Hamamatsu R928 photomultiplier (PMT) detector. Emission from the samples was passed through a detection monochromator positioned 90° to the excitation beam with excitation and emission slit widths of 2.5 mm (band-pass of 5 nm) and 0.5 mm (band-pass of 1 nm), respectively. A spectral scan of a solvent blank was also taken under the same experimental conditions and was subtracted from the spectral trace of the sample. The fluorescence excitation spectra of the complexes were detected at the chlorophyll emission bands near 680 nm with excitation and emission slit widths of 0.5 mm (band-pass of 1 nm) and 2.5 mm (band-pass of 5 nm), respectively. All excitation spectra were corrected for the instrument response by dividing by a calibrated lamp/excitation monochromator profile generated by a built-in photodiode.

Two-Photon Excitation Spectroscopy. Two-photon excitation (TPE) spectra of the complexes were taken using the spectrometer previously described by Shima *et al.* (*19*).

Transient Absorption Spectroscopy. For time-resolved absorption spectroscopy, the samples of MFPCP and HSPCP were resuspended in 50 mM Tricine/20 mM KCl buffer (pH 7.5) containing 60% glycerol and frozen at 20 K using a closed-cycle helium cryostat (APD Cryogenics). The absorbance of the sample in the cell was ∼0.4 per 0.12 cm at the peak of the Chl *a* Q_y absorption band. Transient absorption difference spectra of MFPCP and HSPCP at 20 K were recorded using the femtosecond spectrometer described previously (*30*). The samples were excited at 666 and 677 nm with 200 fs laser pulses (fwhm = 4.5 nm), and the transient absorption spectra were recorded on 100 ps time scales in the 600−750 nm spectral region with a 100 fs step. The kinetic data were corrected for dispersion, and decay-associated spectra (DAS) were constructed on the basis of the global multiexponential fit of the kinetic traces.

Spectral Analysis. The analysis and deconvolution of the absorption spectra of the complexes were carried out using Origin version 7.0.

RESULTS

Absorption Spectroscopy. The absorption spectra of the MFPCP and HSPCP complexes taken at room temperature and 10 K are shown in Figure 2. At room temperature, the primary differences between the spectra of the two different

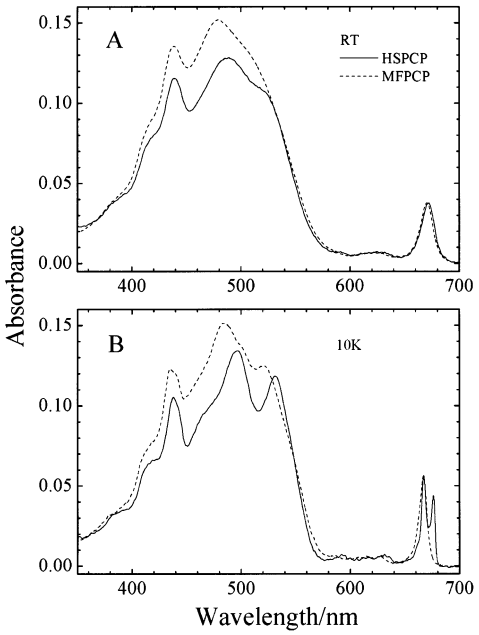

FIGURE 2: Absorption spectra of the MFPCP and HSPCP complexes taken at (A) room temperature and (B) 10 K. The spectra were normalized to the most prominent band in the Chl Q_y absorption region.

complexes are as follows. The ratio of the peridinin absorption at ∼500 nm to the Chl Q_y band at ∼670 nm is smaller for the HSPCP complex than for the MFPCP complex, and the Chl Q_y band of the HSPCP complex is red-shifted by 2 nm compared to that of MFPCP. Also, the absorption maximum of the peridinin in the 450−550 nm region in the HSPCP is red-shifted by 9 nm, and HSPCP shows a more pronounced shoulder on the red edge of the peridinin absorption near 520 nm than does MFPCP. At 10 K, the absorption bands from both complexes display additional distinguishing features. The Chl Q_y region from the HSPCP complex is split into two distinct bands with maxima at 667 and 676 nm. A small shoulder is also evident on the high-energy side of the 667 nm component. The Chl Q_y region from the MFPCP complex exhibits only one prominent peak with a shoulder on the high-energy side; the maximum of the peridinin absorption in the 450−550 nm region is red-shifted by 12 nm in the HSPCP complex compared to the MFPCP complex, and the vibronic features of the peridinin absorption bands are significantly better resolved for the HSPCP complex than for the MFPCP complex.

For comparative purposes and also for use in the analysis of the absorption spectra of the protein complexes, the spectra of Chl *a* and peridinin were recorded at 10 K in 2-MTHF which forms a clear glass at that temperature. These spectra are given in Figure 3A. The Q_y region of the Chl absorption spectrum can be understood and reproduced by a simple summation of two Gaussian components built on a broad baseline (Figure 3B). This is characteristic of Chl solution spectra in this region (*31*). In the 400−600 nm region, linear combinations of the spectra from the individual pigments (Figure 3A) were used to generate the absorption spectral line shapes of the complexes. The Chl *a* components were allowed to have any intensity and wavelength in the fit. The peridinin spectra were allowed to vary with respect to wavelength, but were restricted to having identical intensities. For the MFPCP complex, two Chl *a* and eight peridinin

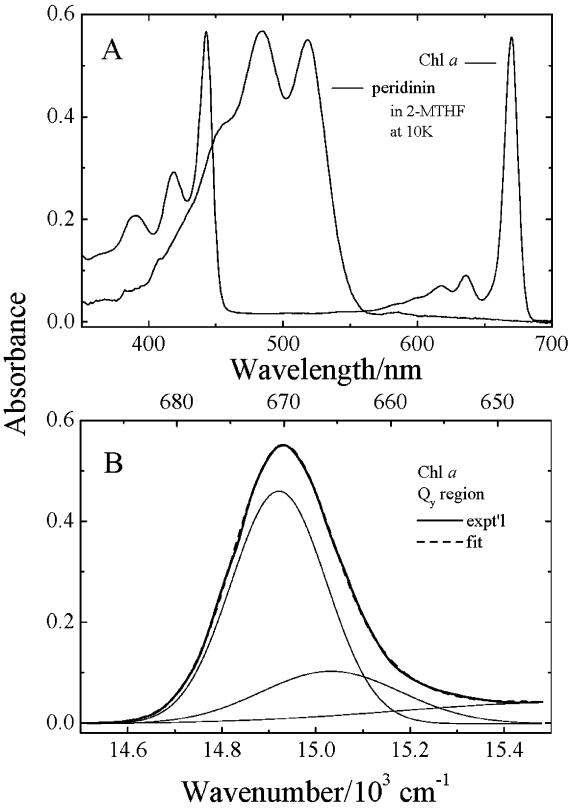

FIGURE 3: (A) Absorption spectra of Chl *a* and peridinin in 2-MTHF at 10 K. (B) Gaussian deconvolution of the Q_y region of the Chl *a* absorption band. The dashed line represents the sum of two Gaussian components having the following intensities, fwhm, and positions: 0.4650, 236.99 cm^{-1}, and 14 921 cm^{-1}, respectively, for peak 1 and 0.1044, 348.93 cm^{-1}, and 15 032 cm^{-1}, respectively, for peak 2.

spectra were used (Figure 4A). For the HSPCP complex, two Chl *a* and six peridinin spectra were used (Figure 4B), in keeping with the results from the stoichiometric analysis (*29*). As mentioned in the introductory section and described in detail previously (*19*), the spectrum of the MFPCP complex is best fit using two blue-shifted peridinins, and three separate pairs of peridinin spectra (Figure 4A). Two Chl *a* spectra having different intensities in the Soret bands at 434 and 439 nm were also required. Fitting the HSPCP spectrum, however, required only one blue-shifted peridinin summed with five equivalent longer wavelength-absorbing peridinins (Figure 4B). Two Chl *a* spectra with different intensities in the Soret bands at 436 and 441 nm were also used.

In the Q_y region, the 10 K absorption spectral profiles of both complexes were fit using Gaussian functions having different amplitudes, positions, and widths (Figure 4C,D). The spectrum from the MFPCP complex was best fit using four Gaussians on a broad absorption background (Figure 4C). The 10 K absorption spectrum from the HSPCP complex in this region also required four Gaussian components built on a broad absorption background (Figure 4D), but the functions were much more clearly resolved in the HSPCP complex than in the MFPCP complex. The parameters characterizing the Gaussian functions are given in the legend of Figure 4.

Fluorescence Spectroscopy. The fluorescence spectra of the HSPCP and MFPCP complexes recorded at room temperature are very similar to each other and to that of Chl *a* in 2-MTHF (Figure 5A). The three spectra display a prominent line near 670 nm and lower-energy, slightly structured, broad vibronic features centered around 725 nm. The peak maxima of the fluorescence spectra of the MFPCP and HSPCP complexes are shifted by 5 and 6 nm, respectively, compared to those of the Chl *a* spectrum (Figure 5A). At 77 K, the three spectra narrow considerably compared to the room temperature spectra, and distinct differences between them are observed (Figure 5B). The 77 K fluorescence spectrum of Chl *a* in 2-MTHF has a maximum at 671 nm and a full width at half-maximum (fwhm) of 15 nm. The MFPCP complex shows its most prominent band at 669 nm and has a fwhm value of 9 nm which is narrower than that of Chl *a*, but not as narrow as that from the HSPCP complex which has its maximum at 675 nm and a fwhm value of 6 nm. A small shoulder on the blue side of the prominent band in the HSPCP complex is also evident. All of the spectra display similarly structured low-energy vibronic features between 700 and 770 nm, although those from HSPCP are red-shifted compared to those from the MFPCP complex (Figure 5B).

The fluorescence excitation spectra recorded at room temperature and 77 K of the two different complexes are shown in Figure 6 overlaid with their $1 - T$ spectra, where T is transmittance. The fluorescence excitation spectra were normalized to the $1 - T$ spectra in the Q_y region for purposes of comparison. The Chl fluorescence was monitored at 730 nm for the figure, but the fluorescence excitation spectra detected at 675, 690, 710, and 720 nm all exhibited identical line shapes. The strong agreement between the fluorescence excitation and $1 - T$ spectral line shapes in the peridinin (450−570 nm) region indicates high (>95%) peridinin-to-Chl energy transfer efficiencies for both complexes at room temperature and 77 K.

Transient Absorption Spectroscopy. Transient difference absorption spectra of the MFPCP and HSPCP complexes recorded at 20 K are shown in Figure 7. Upon excitation of the MFPCP complex into the Q_y absorption band of Chl *a* at 666 nm with spectrally narrow (fwhm = 4.5 nm) 200 fs laser pulses, rapid photobleaching of the Chl Q_y band at the excitation wavelength is observed. The spectral profile of the photobleaching at early times (between 0 and 1 ps) follows the convolution of the pump and probe pulses and did not show any sub-picosecond excitation dynamics (not shown). Figure 7A shows that as time elapses from 1.2 to 99.6 ps, the difference spectrum shifts by 1 nm to the red and narrows slightly. The kinetic traces in Figure 8 show a small decay of photobleaching upon detection at 667 nm (Figure 8A) and an increase in the level of photobleaching detected at 670 nm (Figure 8B) occurring on a picosecond time scale and observed on the background of long-lived photobleaching characteristic of antenna Chls.

The excitation dynamics of HSPCP under similar conditions are significantly different (Figure 7B). A rapid photobleaching of the blue-absorbing Chl *a* spectral form upon excitation at 666 nm is observed. However, the transient spectra detected at pump−probe delays later than 1 ps clearly indicate a decay of photobleaching of this species accompanied by the onset of photobleaching of the spectrum of the red-absorbing Chl component in HSPCP. Panels C and D of Figure 8 show the kinetic traces associated with these absorption changes. Figure 8C shows a substantial

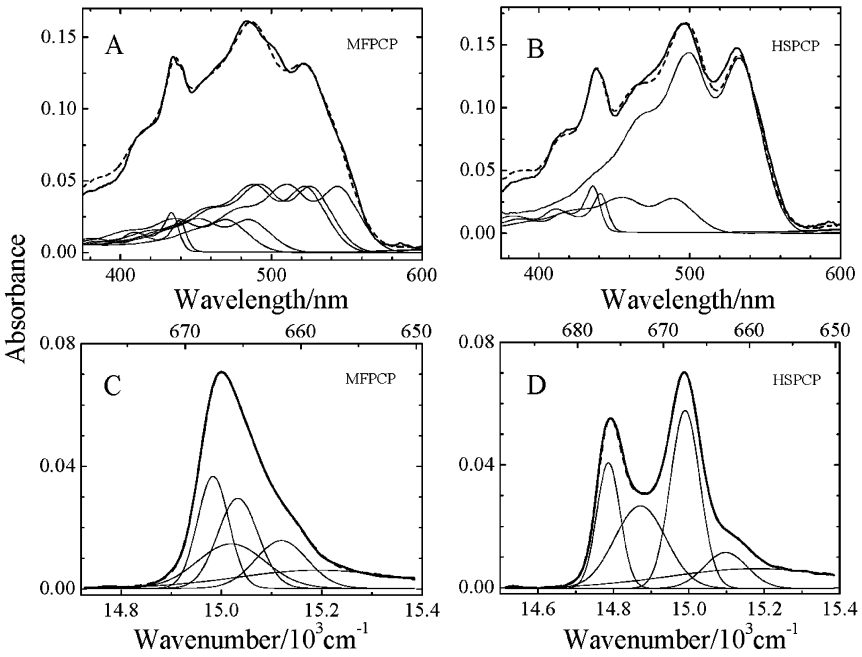

FIGURE 4: Analysis of the 10 K absorption spectra (solid thick lines) of the (A) MFPCP and (B) HSPCP complexes in the 375−600 nm region. The analysis in this region was done by summing the individual spectra (solid thin lines) of Chl *a* and peridinin given in Figure 3. Also shown are deconvolutions of the 10 K spectra in the Q_y region of the (C) MFPCP and (D) HSPCP complexes using Gaussian functions (dashed lines) having the following intensities, fwhm, and positions: 0.04019, 66.53 cm^{-1}, and 14 983 cm^{-1}, respectively, for peak 1; 0.01474, 155.57 cm^{-1}, and 15 019 cm^{-1}, respectively, for peak 2; 0.03095, 89.528 cm^{-1}, and 15 032 cm^{-1}, respectively, for peak 3; and 0.01599, 117.57 cm^{-1}, and 15 119 cm^{-1}, respectively, for peak 4 in MFPCP and 0.04506, 66.19 cm^{-1}, and 14 786 cm^{-1}, respectively, for peak 1; 0.02734, 157.42 cm^{-1}, and 14 871 cm^{-1}, respectively, for peak 2; 0.06141, 87.37 cm^{-1}, and 14 990 cm^{-1}, respectively, for peak 3; and 0.01197, 130.22 cm^{-1}, and 15 097 cm^{-1}, respectively, for peak 4 in HSPCP.

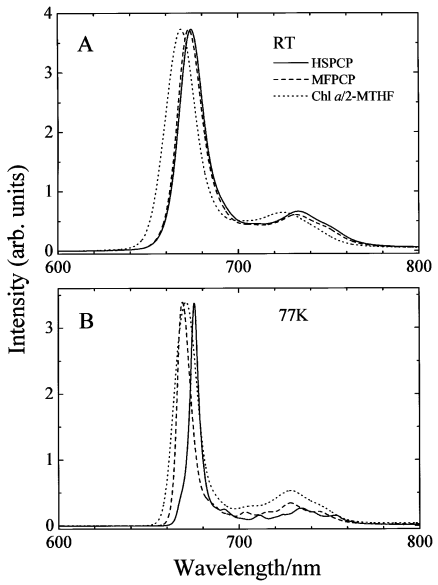

FIGURE 5: Fluorescence spectra of the MFPCP and HSPCP complexes in a buffer/glycerol solution and Chl *a* in 2-MTHF at (A) room temperature (RT) and (B) 77 K. The spectra were normalized to their λ_{max} values.

decay of the photobleaching monitored at 667 nm that is concomitant with the onset of photobleaching monitored at 677 nm (Figure 8D).

Results of global analysis of the transient absorption data are shown in Figure 9. Figure 9A illustrates DAS obtained for MFPCP. The data are best fit with an exponential component having a lifetime of 6.8 ps and a long-lived nondecaying component. Despite the substantial overlap of two Chl spectral forms, the shape of the 6.8 ps DAS is indicative of intraband energy transfer revealing two Chl *a* spectral forms in MFPCP. A split of the Chl Q_y absorption bands in HSPCP (Figure 4D) significantly changed the excitation profile compared to that of MFPCP. Global analysis of the transient data for HSPCP (Figure 9B) revealed DAS with a lifetime of 20 ps and a nondecaying component reflecting the long-lived excitation predominantly localized on the low-energy spectral form of Chl. A 20 ps DAS has a conservative shape for its energy transfer component, indicating an efficient energy transfer from the higher-energy-absorbing Chl to the lower-energy-absorbing Chl. No sub-picosecond excitation dynamics were observed for either of the complexes. The analyses of the dynamics of both complexes reveal one nondecaying long-lived component, which has a maximum at 667 nm for the MFPCP complex and at 675 nm for the HSPCP complex.

The transient difference spectra of the HSPCP complex after excitation at 677 nm with pump−probe delays of 1.2 and 50 ps are shown in Figure 10. The similarity of these spectra and the fact that the maximum of the ΔA is blue shifted relative to the excitation wavelength (fwhm = 95 cm^{-1}) indicate that the red-shifted Chl is the site of excited state energy localization.

Two-Photon Spectroscopy. As observed previously for the TPE spectrum of the MFPCP complex (*19*, *20*), the spectrum of HSPCP overlaps considerably with its one-photon absorption spectrum (Figure 11). The TPE spectrum shown in Figure 11 was generated from the average of three scans using linearly polarized excitation. In the TPE spectrum of MFPCP previously reported (*19*), there is an apparent red edge shoulder at ~550 nm, interpreted as a low-energy vibronic band associated with the red-most absorbing pair

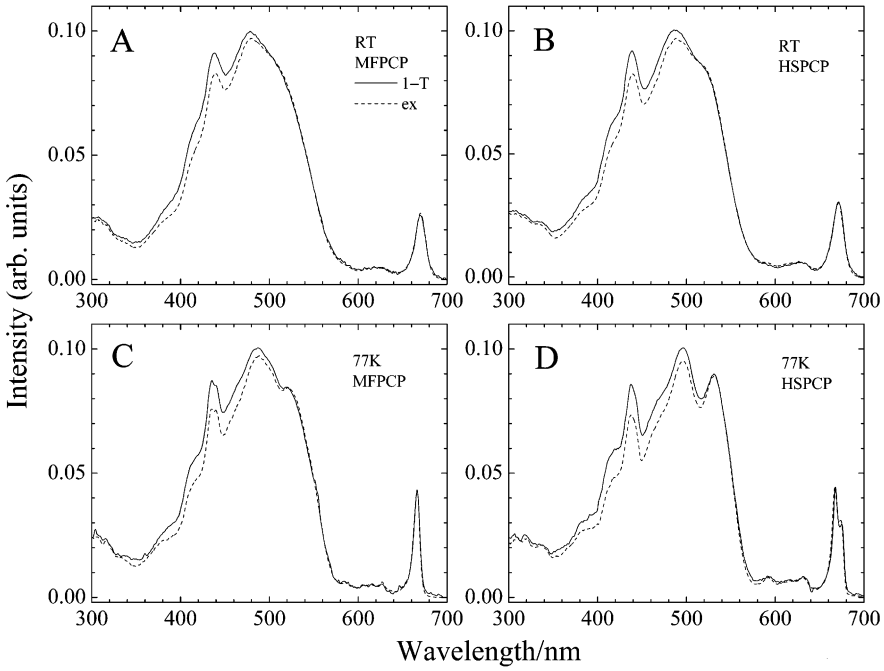

FIGURE 6: Overlay of the fluorescence excitation (ex) and $1 - T$ (T is transmittance) spectra of (A) MFPCP and (B) HSPCP at room temperature (RT) and (C and D) 77 K. The wavelength of detection for the excitation spectra was 730 nm for both MFPCP and HSPCP at RT and 77 K. The intensities of the fluorescence excitation spectra were adjusted to correspond to the $1 - T$ spectra in the Q_y region.

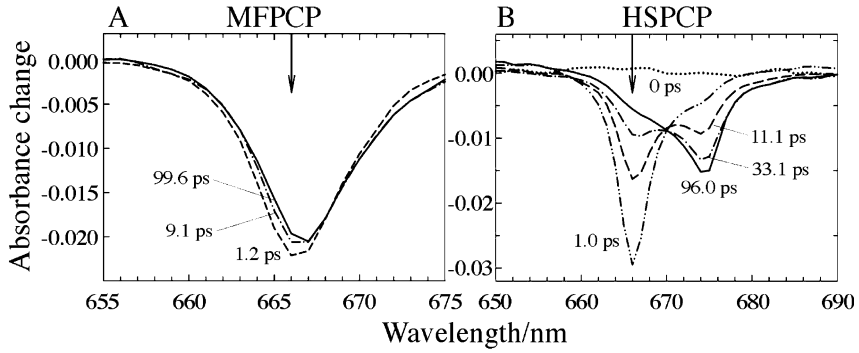

FIGURE 7: Transient difference absorption spectra of (A) MFPCP and (B) HSPCP measured at 20 K with excitation at 666 nm (shown by arrow). In panel A, the ΔA spectra 1.2, 9.1, and 99.6 ps after the excitation are shown. In panel B, the ΔA spectra 0, 1.0, 11.1, 33.1, and 96.0 ps after the excitation are shown. The spectral width of the excitation pulse (fwhm) is 4.5 nm (95 cm^{-1}).

of peridinin molecules. This feature is not present in the HSPCP TPE spectrum reported here.

DISCUSSION

The most obvious difference in the absorption spectra from the two different complexes taken at room temperature is that the amplitude of the absorption in the peridinin region is smaller for HSPCP than for MFPCP. This is due to the fact that the HSPCP complex has six bound peridinins per two Chls whereas the MFPCP has eight peridinins per two Chls. The interpretation of the more subtle changes in the absorption spectra, e.g., the shifting of the peridinin absorption maximum, the different amounts of vibronic structure in the peridinin region, and the shifting of the Chl Q_y band, benefits from the use of cryogenic temperatures.

The 10 K absorption spectrum of the MFPCP complex in a buffer/glycerol glass (Figure 4A) can be fit in the 400−600 nm region using a linear combination of Chl *a* and peridinin solution spectra (Figure 3) as components. The procedure of allowing the Chl *a* components to have any intensity and restricting the peridinin spectra to the same intensity does not yield a perfect fit because of pigment−

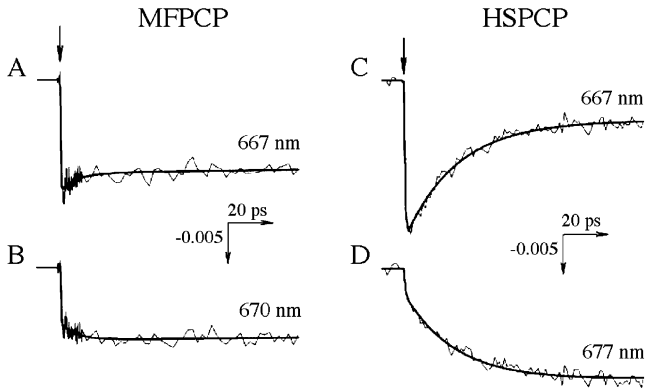

FIGURE 8: Transient kinetics of absorption changes in (A and B) MFPCP and (C and D) HSPCP measured at 20 K with excitation at 666 nm (shown with an arrow in Figure 7). The detection wavelengths are specified in the figure. The thick solid lines represent fits based on a multiexponential model (see Figure 9 for the decay-associated spectra).

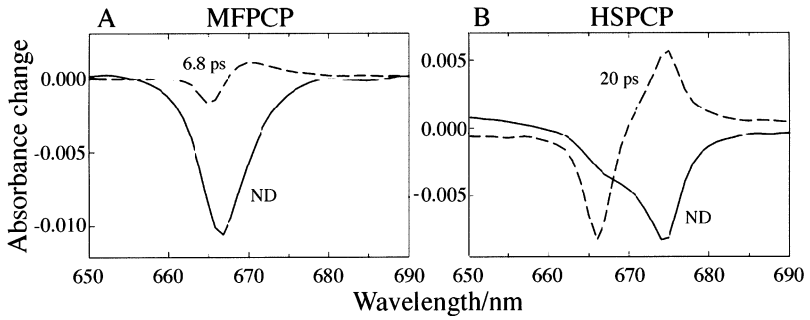

FIGURE 9: Decay-associated spectra obtained after global analysis of the transient kinetics of absorption changes in the (A) MFPCP and (B) HSPCP complexes detected at 20 K after excitation at 666 nm. No sub-picosecond excitation dynamics were observed for either of the complexes. The best fits were obtained with one energy transfer component (6.8 ps for MFPCP and 20 ps for HSPCP) and a long-lived, nondecaying (ND) component.

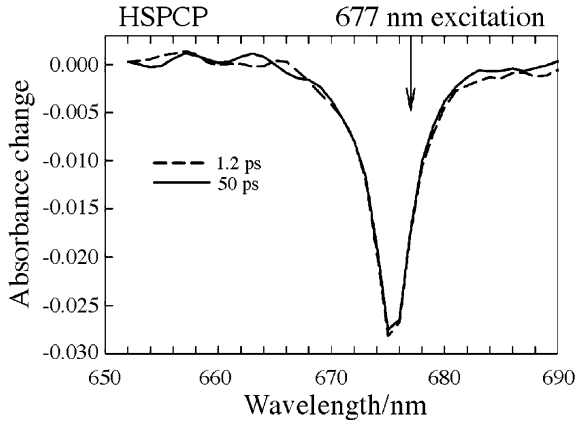

FIGURE 10: Transient difference absorption spectra of the HSPCP complex measured at 20 K with excitation at 677 nm. The ΔA spectra are shown at pump−probe delays of 1.2 and 50 ps. Note that the ΔA maximum is blue-shifted relative to the excitation pulse which has a fwhm of 95 cm^{-1}. The absence of a time evolution of this signal indicates this Chl is the site of energy localization.

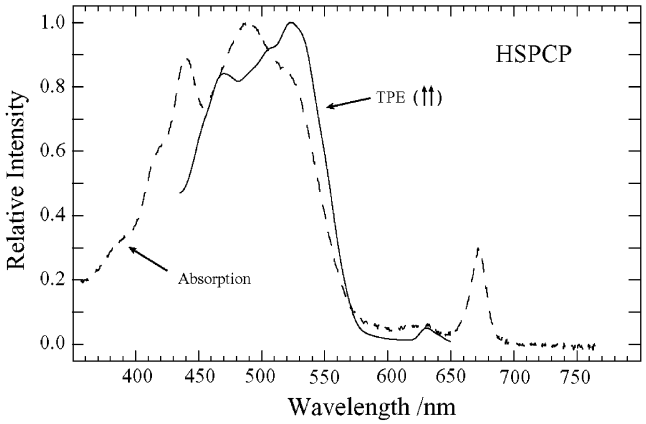

FIGURE 11: Two-photon excitation (TPE) spectrum using parallel light polarization of HSPCP at room temperature overlaid with its one-photon absorption spectrum (dashed line). The TPE signal is the average of three scans using linearly polarized excitation.

pigment and pigment−protein interactions and site energy differences between the protein and the 2-MTHF solvent, but the simulated absorption profile is unique and reproduces most of the spectral features. The most important result is that the simulation of the MFPCP spectrum requires two peridinin molecules to be significantly blue-shifted relative to the other six which are ascribed to three different pairs. Our previous experimental and computational work (*19*) has suggested that these two peridinin molecules occupy positions 612 and 622 within the PCP (Figure 1), and that these molecules have inverted S_1 and S_2 energies. Damjanovic *et al.* (*10*) have suggested that the peridinin molecules occupying positions 612 and 622 do not transfer energy directly to the chlorophyll molecules, but rather to the other peridinins in the protein. Our prediction that the level ordering is reversed in peridinins 612 and 622 would enhance dipolar coupling of these molecules with the other peridinin molecules (*19*). Unfortunately, the MNDO-PSDCI calculations were not able to assign with confidence which peridinins in the structure give rise to the red-most absorption (shoulder) near 550 nm. This absorption feature is not seen in the 10 K spectrum of the HSPCP complex (Figure 4B), nor is it seen in its TPE excitation spectrum (Figure 11). However, both MFPCP and HSPCP display strong overlap between their TPE and one-photon absorption profiles. As discussed in detail previously (*19*), this is indicative of type II processes which, because of the presence of a large oscillator strength for the one-photon transition coupled with a significant change in the dipole moment upon excitation, lead to enhancement in the probability of two-photon absorption. In this regard, the MFPCP and HSPCP complexes are very similar.

The spectral line shapes of MFPCP and HSPCP can be simulated with high precision using only the solution spectra of the pigments as components. This suggests that the primary source of the spectral heterogeneity of the peridinins in the protein is a variation in site energies sufficient in magnitude to alter the energies, but not the line shapes, of the ground state-to-$1^1B_u^+$ transitions. The analysis of the absorption spectra indicates that the site energy distribution of the peridinins is broader for the MFPCP than for the HSPCP complex. This is corroborated by the CD spectra of the two complexes which show an ∼25% larger line width in the peridinin region for the MFPCP than for the HSPCP complex (*29*). A good fit to the 10 K absorption spectrum of the HSPCP complex is achieved using five spectrally equivalent peridinins having spectral origins at ∼530 nm and only one blue-shifted peridinin molecule having a spectral origin at ∼490 nm. Unlike the MFPCP, none of the peridinins in the HSPCP is red-shifted to 550 nm.

The fact that the HSPCP has six peridinins, versus MFPCP which has eight, makes it tempting to suggest that two symmetric peridinins from the MFPCP structure, perhaps per612 and per622, have been lost in the HSPCP structure. However, because the sequence of HSPCP is only 31%

homologous with that of MFPCP, the two protein structures are likely to be significantly different. Thus, it would be an oversimplification to state that the differences in spectral properties between the complexes can be accounted for solely by two peridinin molecules being removed from MFPCP to form HSPCP. Also, it would be difficult to understand how the removal of two symmetrically distributed peridinins from MFPCP would result in a complex that still has one blue-shifted peridinin and asymmetry in the Chl binding sites that is sufficient to cause the pronounced splitting of the Chl Q_y bands (Figure 4D).

The Gaussian deconvolution of the Chl *a* absorption spectrum recorded at 10 K in a 2-MTHF glass (Figure 3B) provides a guide to what one should expect for the spectra of the pigment−protein complexes in the Q_y region. The solution spectrum of Chl *a* in this region shows a prominent spectral origin at 670 nm and a broad zero-phonon line centered at 665 nm, consistent with the spectral analysis carried out previously for chlorophylls (*32*). The deconvolution of the 10 K spectra of MFPCP (Figure 4C) and HSPCP (Figure 4D) shows features similar to those observed in solution, viz., single prominent spectral origins for both bound Chls, each of which is accompanied by a zero-phonon line at higher energy. The profound splitting of the Chl Q_y bands observed in the HSPCP spectra is suggestive of a major perturbation in the symmetry of the two Chls in the two subunit domains compared to the MFPCP spectra which, as suggested above, could have resulted from the removal of two peridinins *and* structural differences between the two protein complexes.

Again, because the structure of the HSPCP complex is not known, the possibility exists that exciton coupling between the Chls could be responsible for the splitting of the Q_y bands. The relatively long Chl center-to-center distance of 17.4 Å for the Chls in the MFPCP complex leads to a relatively small ($\sim$7 cm^{-1}) exciton coupling between the molecules (*11*). This interaction is adequate to ensure efficient energy transfer, but not large enough to perturb the absorption spectra of the pigments. If the distance between Chls is comparable in HSPCP and MFPCP, the exciton coupling will also not be of sufficient magnitude to split the Q_y bands. We have examined this issue using transient optical spectroscopy to monitor the time course of the photobleaching occurring after selective excitation of the Chl molecules. The results will be discussed below.

The fluorescence spectra of MFPCP, HSPCP, and Chl *a* in solution (Figure 5) are all very similar and typical of monomeric Chl species. Except for minor wavelength differences, the spectra taken at room temperature are virtually identical. At 77 K, however, each spectrum has a significantly different position and line width, suggestive of different site energies for the Chls. The spectrum of Chl *a* in 2-MTHF narrows and shifts by $\sim$3 nm to the red upon cooling from room temperature to 77 K, but the spectrum of Chl *a* in MFPCP narrows and shifts by $\sim$4 nm to the blue. Neither of these changes is as dramatic as the observation that upon cooling the HSPCP complex to 77 K, where the splitting of the Q_y bands is evident (Figure 6D), only one of the two Q_y absorption bands has an associated fluorescence line. This suggests that energy absorbed by the blue-shifted Chl at 667 nm is rapidly transferred to the red-absorbing Chl at 676 nm which traps the excitation. This hypothesis also has been explored by transient absorption experiments and will be discussed below.

The overlay of the fluorescence excitation spectra with the $1 - T$ spectra for both the MFPCP and HSPCP complexes (Figure 6) indicates a very high (>95%) peridinin-to-Chl energy transfer efficiency. In both complexes, there is a slight decrease in energy transfer efficiency as shorter wavelengths of excitation are employed in the peridinin region. This indicates that the spectrally distinct peridinins are transferring energy to the Chls with different efficiencies. Akimoto *et al.* (*2*) also noticed that the peridinin-to-Chl energy transfer efficiency was dependent on excitation wavelength. The blue-shifted peridinins are suggested by this result to be less efficient at transferring energy to the Chls than the red-shifted peridinins. This effect is also seen at cryogenic temperatures (Figure 6C,D), where the MFPCP and HSPCP complexes are seen to be similarly efficient at peridinin-to-Chl energy transfer.

As mentioned above, transient absorption experiments provide the means of examining whether the splitting between the Q_y bands of the Chls observed in the low-temperature absorption spectra of the HSPCP complex arises from exciton coupling. The experiments also allow an examination of whether the low-energy Chls in both complexes act as traps of excitation energy.

The time course of the transient absorption spectra presented in Figure 7 clearly shows sequential Chl-to-Chl energy transfer in both MFPCP and HSPCP complexes. Selective excitation of the higher-energy-absorbing Chl in either MFPCP or HSPCP results in an instantaneous photobleaching of only that absorption band. This clearly indicates that exciton coupling is not the reason for the splitting of the Q_y bands observed in the absorption spectrum of HSPCP at low temperatures. Undoubtedly, the origin of the splitting is the different site energies of the Chls. In both complexes, the onset of the photobleaching of the red-shifted Chl occurs concomitantly with the decay of the photobleaching of the blue-absorbing Chl, and in the HSPCP, selective excitation of the red-shifted Chl does not result in a photobleaching of the blue-absorbing Chl (Figure 10). These results clearly depict downhill energy transfer occurring between weakly coupled Chl molecules in both complexes.

The question of why transfer of energy from Chl to Chl is a factor of 2.9 (20 ps compared to 6.8 ps) slower in HSPCP than in MFPCP remains. This may be rationalized within the context of the Förster model of energy transfer which has found wide-ranging applicability as a singlet-energy transfer mechanism between weakly coupled pigments (*33*).

According to the Förster model, the rate of excitation energy transfer is given by

$$k_{DA} = c\frac{\kappa^2 k_r^D}{r^6 n^4}\int \frac{\epsilon_A(\tilde{\nu}) f_D(\tilde{\nu})}{\tilde{\nu}^4}\, d\tilde{\nu} \qquad (1)$$

where c is a constant, n is the refractive index, r is the center-to-center distance between the pigments, k_r^D is the radiative rate constant of the energy donor, ϵ_A corresponds to the absorption of the acceptor on a wavenumber (cm^{-1}) scale, f_D represents the fluorescence spectrum of the donor on a wavenumber scale, and κ is the orientation factor of the

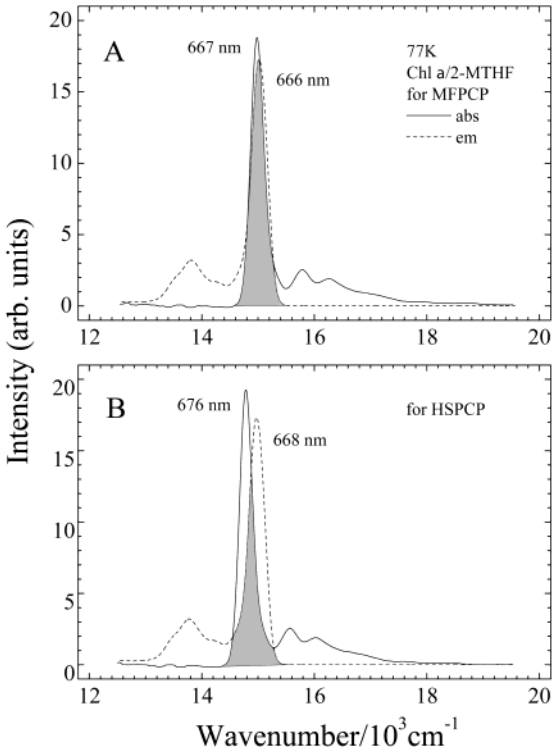

FIGURE 12: Spectral overlap (shaded region) between the absorption and emission profiles of Chl *a* recorded in 2-MTHF at 77 K and corresponding to the absorption and fluorescence spectra of the (A) MFPCP and (B) HSPCP complexes. The Chl *a* emission spectra were shifted to correspond to the position of the λ_{max} of the higher-energy Chl, and the absorption spectra were shifted to correspond to the maximum absorption of the low-energy Chl in each complex. The positions of these lines were based on the Gaussian deconvolutions of the Q_y region for each complex shown in Figure 4 (C and D). The ratio between the values of the spectral overlap of the MFPCP and HSPCP line shapes is 1.4 and accounts in part for the slower dynamics of Chl-to-Chl energy transfer in the HSPCP vs that in MFPCP (Figures 7−9).

electronic coupling term given by

$$\kappa = \boldsymbol{\mu}_D \cdot \boldsymbol{\mu}_A - 3(\boldsymbol{\mu}_D \cdot r)(\boldsymbol{\mu}_A \cdot r) \quad (2)$$

where $\boldsymbol{\mu}_D$ and $\boldsymbol{\mu}_A$ are the transition moment unit vectors for the donor and acceptor molecules, respectively.

There are three factors that could account for the change in the rate of energy transfer upon going from MFPCP to HSPCP: spectral overlap, distance *r*, and orientation κ. The index of refraction of the protein and the radiative rate constant for the protein-bound Chl *a* donor molecules are not expected to be significantly different for the two pigment−protein complexes.

Figure 12 uses the 77 K absorption and fluorescence spectra of Chl *a* in 2-MTHF to compute spectral overlap values for the Chls at the wavelengths corresponding to absorption and fluorescence in the MFPCP and HSPCP complexes which may then be compared directly. Figure 12A shows the spectral overlap for MFPCP where the maxima in the fluorescence spectrum of the higher-energy Chl donor and the absorption spectrum of the red-absorbing Chl acceptor occur at 666 and 667 nm, respectively. Figure 12B shows there is less overlap for HSPCP where the fluorescence maximum of the Chl donor occurs at 668 nm while the absorption maximum of the Chl acceptor occurs at 676 nm. The ratio of the spectral overlap integrals of the MFPCP and HSPCP complexes computed from the spectra given in Figure 12 is 1.4. Therefore, although a difference in spectral overlap may be part of the reason why the energy transfer between the Chls in HSPCP is slower than in MFPCP, it cannot completely account for the factor of 2.9 change in dynamics that is observed.

The remaining factor of 2.9/1.4 (=2.1) in the rates could arise from differences in the distance between the Chls in the MFPCP and HSPCP complexes. If one assumes that the orientation (κ factor) of the Chls is the same for the two complexes, the power of six dependence on distance would require that the center-to-center separation between the Chls in HSPCP increase from 17.4 Å, its value in MFPCP, to 19.7 Å. However, the slower rate may also be due to different orientations between the pigments.

The crystal structure of MFPCP has revealed the angle between the Q_y absorption transition moments of the two Chls to be 79.7°. The value of κ^2 computed using this angle and the angles (83.6° and 96.5°) between the Q_y transitions and the intermolecular axis, *r*, is 0.0469. If one assumes that the center-to-center distance between the Chls is the same in both complexes, accounting for the remaining factor of 2.1 slower dynamics for the HSPCP complex requires that κ^2 be changed to 0.0224. This would mean that if the angle between the Q_y's of the Chls and *r* remained constant, the angle between the two Q_y's would have to change from 79.7° to 83.6° to account for the slower dynamics in the HSPCP complex. This is a very small change and entirely reasonable. Alternatively, reorientation of the Chl Q_y's with respect to the intermolecular axis, *r*, could bring about a decrease in the rate of energy transfer. However, without more detailed structural information, it is not possible to state whether distance or geometric factors (or both) are the most important in causing the change in the rate of Chl-to-Chl energy transfer between the complexes. Structural studies of crystallized HSPCP are ongoing.

ACKNOWLEDGMENT

We thank Drs. Richard Cogdell, Tomás Polívka, and Eckhard Hofmann for several useful discussions.

REFERENCES

1. Song, P.-S., Koka, P., Prézelin, B. B., and Haxo, F. T. (1976) *Biochemistry 15*, 4422−4427.
2. Akimoto, S., Takaichi, S., Ogata, T., Nishimura, Y., Yamazaki, I., and Mimuro, M. (1996) *Chem. Phys. Lett. 260*, 147−152.
3. Bautista, J. A., Hiller, R. G., Sharples, F. P., Gosztola, D., Wasielewski, M., and Frank, H. A. (1999) *J. Phys. Chem. A 103*, 2267−2273.
4. Krueger, B. P., Lampoura, S. S., van Stokkum, I. H. M., Papagiannakis, E., Salverda, J. M., Gradinaru, C. C., Rutkauskas, D., Hiller, R. G., and van Grondelle, R. (2001) *Biophys. J. 80*, 2843−2855.
5. Hofmann, E., Wrench, P. M., Sharples, F. P., Hiller, R. G., Welte, W., and Diederichs, K. (1996) *Science 272*, 1788−1791.
6. Hiller, R. G. (1999) in *The Photochemistry of Carotenoids* (Frank, H. A., Young, A. J., Britton, G., and Cogdell, R. J., Eds.) pp 81−98, Kluwer Academic Press, Dordrecht, The Netherlands.
7. Carbonera, D., Giacometti, G., Segre, U., Angerhofer, A., and Gross, U. (1999) *J. Phys. Chem. B 103*, 6357−6362.
8. Ritz, T., Damjanovic, A., Schulten, K., Zhang, J.-P., and Koyama, Y. (2001) *Photosynth. Res. 66*, 125−144.
9. Zigmantas, D., Polivka, T., Hiller, R. G., Yartsev, A., and Sundström, V. (2001) *J. Phys. Chem. A 105*, 10296−10306.

10. Damjanovic, A., Ritz, T., and Schulten, K. (2000) *Biophys. J. 79*, 1695−1705.
11. Kleima, F. J., Wendling, M., Hofmann, E., Peterman, E. J. G., van Grondelle, R., and van Amerongen, H. (2000) *Biochemistry 39*, 5184−5195.
12. Kleima, F. J., Hofmann, E., Gobets, B., Van Stokkum, I. H. M., Van Grondelle, R., Diederichs, K., and Van Amerongen, H. (2000) *Biophys. J. 78*, 344−353.
13. Carbonera, D., Giacometti, G., and Segre, U. (1995) in *Photosynthesis: from Light to Biosphere* (Mathis, P., Ed.) Vol. IV, pp 147−150, Kluwer, Montpellier, France.
14. Osaka, A., and Kume, T. (1998) *Tetrahedron Lett. 39*, 655−658.
15. Pilch, M., and Pawlikowski, M. (1998) *J. Chem. Soc., Faraday Trans. 94*, 227−232.
16. Iglesias-Prieto, R., and Trench, R. K. (1996) *J. Plant Physiol. 149*, 510−516.
17. Bautista, J. A., Connors, R. E., Raju, B. B., Hiller, R. G., Sharples, F. P., Gosztola, D., Wasielewski, M. R., and Frank, H. A. (1999) *J. Phys. Chem. B 103*, 8751−8758.
18. Frank, H. A., Bautista, J. A., Josue, J., Pendon, Z., Hiller, R. G., Sharples, F. P., Gosztola, D., and Wasielewski, M. R. (2000) *J. Phys. Chem. B 104*, 4569−4577.
19. Shima, S., Ilagan, R. P., Gillespie, N., Sommer, B. J., Hiller, R. G., Sharples, F. P., Frank, H. A., and Birge, R. R. (2003) *J. Phys. Chem. A 107*, 8052−8066.
20. Zimmermann, J., Linden, P. A., Vaswani, H. M., Hiller, R. G., and Fleming, G. R. (2002) *J. Phys. Chem. B 106*, 9418−9423.
21. Mao, L., Wang, Y., and Hu, X. (2003) *J. Phys. Chem. B 107*, 3963−3971.
22. Vaswani, H. M., Hsu, C.-P., Head-Gordon, M., and Fleming, G. R. (2003) *J. Phys. Chem. B 107*, 7940−7946.
23. Zigmantas, D., Hiller, R. G., Yartsev, A., Sundström, V., and Polivka, T. (2003) *J. Phys. Chem. B 107*, 5339−5348.
24. Zigmantas, D., Hiller, R. G., Polivka, T., and Sundström, V. (2002) *Proc. Natl. Acad. Sci. U.S.A. 99*, 16760−16765.
25. Polívka, T., and Sundström, V. (2003) *Chem. Phys.* (in press).
26. Ogata, T., Kodama, M., Nomura, S., Kobayashi, M., Nozawa, T., Katoh, T., and Mimuro, M. (1994) *FEBS Lett. 356*, 367−371.
27. Iglesias-Prieto, R., Govind, N. S., and Trench, R. K. (1991) *Proc. R. Soc. London, Ser. B 246*, 275−283.
28. Iglesias-Prieto, R., and Trench, R. K. (1997) *Mar. Biol. 130*, 23−33.
29. Sharples, F. P., Wrench, P. M., Ou, K., and Hiller, R. G. (1996) *Biochim. Biophys. Acta 1276*, 117−123.
30. Melkozernov, A. N., Lin, S., and Blankenship, R. E. (2000) *Biochemistry 39*, 1489−1498.
31. Shipman, L. L., Cotton, T. M., Norris, J. R., and Katz, J. J. (1976) *J. Am. Chem. Soc. 98*, 8222−8230.
32. Avarmaa, R. A., and Rebane, K. K. (1985) *Spectrochim. Acta 41A*, 1365−1380.
33. Förster, T. (1968) *Ann. Phys. 2*, 55−75.

BI0357964